In Situ–Based Reanalysis of the Global Ocean Temperature and Salinity with ISAS: Variability of the Heat Content and Steric Height

FABIENNE GAILLARD, THIERRY REYNAUD, AND VIRGINIE THIERRY

Ifremer, UMR-6523 LPO, CNRS/Ifremer/IRD/UBO, Plouzané, France

NICOLAS KOLODZIEJCZYK

UBO, UMR-6523 LPO, CNRS/Ifremer/IRD/UBO, Plouzané, France

KARINA VON SCHUCKMANN

Mediterranean Institute of Oceanography, Marseille, France

(Manuscript received 7 January 2015, in final form 26 November 2015)

ABSTRACT

The In Situ Analysis System (ISAS) was developed to produce gridded fields of temperature and salinity that preserve as much as possible the time and space sampling capabilities of the Argo network of profiling floats. Since the first global reanalysis performed in 2009, the system has evolved, and a careful delayed-mode processing of the 2002–12 dataset has been carried out using version 6 of ISAS and updating the statistics to produce the ISAS13 analysis. This last version is now implemented as the operational analysis tool at the Coriolis data center. The robustness of the results with respect to the system evolution is explored through global quantities of climatological interest: the ocean heat content and the steric height. Estimates of errors consistent with the methodology are computed. This study shows that building reliable statistics on the fields is fundamental to improve the monthly estimates and to determine the absolute error bars. The new mean fields and variances deduced from the ISAS13 reanalysis and dataset show significant changes relative to the previous ISAS estimates, in particular in the Southern Ocean, justifying the iterative procedure. During the decade covered by Argo, the intermediate waters appear warmer and saltier in the North Atlantic and fresher in the Southern Ocean than in *World Ocean Atlas 2005* long-term mean. At interannual scale, the impact of ENSO on the ocean heat content and steric height is observed during the 2006/07 and 2009/10 events captured by the network.

1. Introduction

During the previous decades, several observing networks have been set up in the ocean. They are now coordinated within the Global Ocean Observing System (GOOS), the oceanographic component the Global Earth Observing System of Systems (GEOSS; http://www.earthobservations.org). Systematic observation of the global ocean properties was initiated with XBT lines (http://www.jcommops.org/sot/soop/), drifting buoys (http://www.jcommops.org/dbcp/), and fixed-point moorings (http://www.oceansites.org/). However, most measurements were restricted to the tropical band or to the near-surface layers or reported only temperature. In the 2000s, the Argo array of profiling floats extended the concept of systematic observation to the full range of latitudes and toward deeper levels (2000 m), with equal sampling in temperature and salinity (Freeland et al. 2010), and Argo has now become the core of the ocean in situ observing network (http://www.jcommops.org/argo). These networks monitor the upper limb of the ocean with relatively high time resolution, but over a limited number of essential climate variables. They need to be complemented by sustained full-depth and high-accuracy hydrographical measurements (Hood et al. 2010) to cover the full range of ocean climate variability.

The availability of comprehensive observations, with unprecedented time and space sampling, opened the way to a new vision of the ocean state. Monitoring of the

Corresponding author address: Fabienne Gaillard, Ifremer, UMR-6523 LPO, CS 10070, F-29280 Plouzané, France.
E-mail: fabienne.gaillard@ifremer.fr

DOI: 10.1175/JCLI-D-15-0028.1

global ocean is easier when temperature and salinity observations are synthesized and resampled on a regular grid. The methods for interpolating in situ observations have evolved to better use the new data information content, and climate analyses of the global ocean have moved from pentadal images with space resolution barely lower than 1000 km to monthly views at resolution of a few hundreds of kilometers or less. Vertical resolution has improved similarly to reach 1 dam.

Data from the various observing networks are also assimilated in global ocean models that reconstruct the full set of variables describing the ocean state, using the model equations to link the variables observed at limited places in space and time. This type of analysis offers the best synthesis of our knowledge, combining observations with dynamics. However, the assimilation process may lead to reject part of the information provided by the observations if it is considered as incompatible with the model. To facilitate the computation of metrics and evaluate how the model reproduces integral quantities such as heat and salt content, gridded fields obtained by simple interpolation of in situ observations remain a valuable reference. In situ–based gridded statistics, such as the mean state and the variance, are also of importance since all assimilation methods require a priori information on the statistics of the fields.

The National Oceanographic Data Centre (NODC) maintains the World Ocean Database. It assembles all data available to create long-term mean fields [the *World Ocean Atlas* (*WOA*)] and global heat and salt content time series. Until recently, the resolution, limited by data scarceness, was coarse: the *World Ocean Atlas* had a horizontal grid resolution of 1° and 26 levels from 0 to 2000 m (Locarnini et al. 2010). Since Argo started to collect observations in the early 2000s, the network has been gradually extended from the North Atlantic and North Pacific to the global ocean until the nominal number of 3000 floats was reached in the second half of 2007. It then became possible to produce monthly fields for the recent period with horizontal and vertical resolution significantly higher than previously done. The standard Roemmich–Gilson climatology was among the first monthly product based on Argo data (Roemmich and Gilson 2009); it has a slightly increased vertical resolution (58 levels from 0 to 2000 m), the horizontal grid size is 1°, and the covariance scales vary with latitude. Since then, many products have been made available (see the Argo web page: http://www.argo.ucsd.edu/Gridded_fields.html), some of them were included in intercomparison exercises of in situ–based analyses (Chang et al. 2014) or in conjunction with model reanalysis (Balmaseda et al. 2015). The In Situ Analysis System (ISAS) presented here (Gaillard et al. 2009) produces global monthly fields from Argo data merged with observations from other networks on a 0.5° grid and with a vertical resolution of 152 levels from 0 to 2000 m and covariances defined at each grid point. ISAS is developed and used in research mode at the Laboratoire de Physique des Oceans (LPO), in close collaboration with the Coriolis data center, one of the Argo Global Data Assembly Centers (GDACs) that implements proofed versions for operational applications.

Studies of ocean changes from annual to decadal time scales usually involve the definition of a mean state over a reference period that spans 20–30 yr to which a particular state is compared. Recently, the *World Ocean Atlas* has been upgraded for *WOA13*, with 67 levels in the 0–2000-m range (Locarnini et al. 2013) and the long time series available allows NODC to propose decadal or multidecadal averages in addition to the global long-term mean. The Argo dataset has become sufficiently dense to construct climatologies over reference periods; however, the global ocean observing system has not yet reached the canonical 20–30-yr duration, and a strategy has to be defined in order to reevaluate periodically the reference statistics at minimum expenses. We present here a simple way to upgrade the climatologies by simply averaging the monthly products (ISAS-ana) over the selected time period and obtain the mean seasonal cycle (ISAS-clim). The corresponding variances of the dataset relative to this new reference state are also recomputed.

Several studies of the ocean heat content (OHC) and steric height (SH) based on this dataset have been performed in the early stages for the 2003/04–08 period, using Argo data only (Roemmich and Gilson 2009), including CTDs and mooring observations (von Schuckmann et al. 2009), or combining in situ with satellite data (Willis et al. 2008; Chang et al. 2010; Meyssignac and Cazenave 2012). An intent to cover the altimetry era (1993–2008) was done including XBTs (Lyman and Johnson 2008; Lyman et al. 2010). Decadal and interannual variability was revisited for a period starting in the 1950s, based on in situ data alone (Domingues et al. 2008; Levitus et al. 2012) or a combination of in situ measurements, satellite data, and forced model output (Balmaseda et al. 2013). The time series of OHC and SH anomalies obtained by the different teams are similar, indicating that they all capture the same global features of the ocean changes, but they do not fully agree within error bars, which means that these errors are underestimated. The discrepancies can be attributed to the datasets, to the methods, and to the sets of additional information or hypotheses that are needed to obtain a solution.

The general objective of this paper is to present analyzed fields from the global analysis of the period 2002–12 for ISAS (ISAS13) and help the user understand their

potential and limitation. This work is complementary to the intercomparison exercises already carried or planned. We first expose the methodology and the underlying hypothesis and describe the iterative procedure designed to upgrade the products. We present how we deal with the double dataset flux: the globally assembled datasets (GADS) prepared for operational oceanography that contain real-time data on one hand and the platform-oriented datasets (PODS) holding only validated and adjusted data better adapted for scientific and climatological studies on the other hand. The results of a sensitivity test point out the importance of the a priori information provided by the reference state and the corresponding variances, both for the estimate and for the corresponding error. The robustness of the results and error estimates are evaluated on the integral quantities, OHC and SH, at global and regional scales, and we pay particular attention to the period during which the Argo network was building up. Finally, we analyze those results in order to characterize the last decade and obtain insights on the interannual variability.

2. Methodology

ISAS was designed to synthesize the Argo temperature and salinity profiles and produce the corresponding monthly gridded fields to monitor the time evolution of these essential ocean variables. ISAS space and time resolution have been adapted to the Argo array of profiling floats. The main goal is to perform climatic studies and extract meaningful indices; for that reason, the quality control of the data has been a strong concern since the beginning of the processing. To complement the Argo network, ISAS integrates any type of in situ observation from individual profiles to fixed-point time series.

a. Optimal interpolation

The temperature and salinity fields are mapped on a regular grid using the optimal interpolation (OI) technique presented in Bretherton et al. (1976), which we portray here in a formalism close to Ide et al. (1997). The interpolated field is the sum of a reference field (or first guess) and an anomaly obtained as a linear combination of observations through a gain matrix $\mathbf{K}^{\mathrm{OI}}$ that involves covariance matrices:

$$\mathbf{x} = \mathbf{x}_{\mathrm{ref}} + \mathbf{K}^{\mathrm{OI}}(\mathbf{y} - \mathbf{y}_{\mathrm{ref}}), \tag{1}$$

with

$$\mathbf{K}^{\mathrm{OI}} = \mathbf{C}_{\mathrm{ao}}(\mathbf{C}_{\mathrm{oo}} + \mathbf{R})^{-1}, \tag{2}$$

where $\mathbf{x}$ and $\mathbf{y}$ are the vectors of estimated field values at the grid points and observation points, respectively, and $\mathbf{x}_{\mathrm{ref}}$ and $\mathbf{y}_{\mathrm{ref}}$ are the vectors of the reference field values at the grid points and observation points, respectively, and the superscript ref stands for the reference field. In Eq. (2), $\mathbf{C}_{\mathrm{ao}}$ is the covariance matrix between analyzed field at grid points and observations; $\mathbf{C}_{\mathrm{oo}}$ is the covariance matrix of the reference field in the observation space; and $\mathbf{R}$ is the error matrix that includes measurement error and subgrid scales. In the Ide et al. (1997) formalism, the gain matrix is

$$\mathbf{K}^{\mathrm{OI}} = \mathbf{B}\mathbf{H}^{\mathrm{T}}(\mathbf{H}\mathbf{B}\mathbf{H}^{\mathrm{T}} + \mathbf{R})^{-1}. \tag{3}$$

The mapping of matrix $\mathbf{H}$ is not expressed directly in OI but satisfies $\mathbf{B}\mathbf{H}^{\mathrm{T}} = \mathbf{C}_{\mathrm{ao}}$ (Gaillard et al. 2009), and $\mathbf{B}$ is the error covariance matrix of the first guess.

The first implementation of ISAS was made in the Atlantic in the early stages of Argo (Gaillard et al. 2009); since then, the system has been extended to the global ocean and regularly updated to improve the accuracy of the results and the efficiency of the process. We describe here shortly the ISAS tool version 6 (ISAS-V6; Gaillard 2012) that was used to produce ISAS13.

The temperature and salinity fields produced by the ISAS analysis are mapped on a grid with horizontal resolution that follows Mercator projection: $dy = R_{\mathrm{earth}}\cos\theta d\theta_0$. The resolution is equivalent to 0.5° at the equator ($dx = dy = 56$ km); it increases toward higher latitudes but is bounded to 22 km north of 66.5°N. The bathymetry is an interpolation of the 2′ resolution data from ETOPO2 on the ISAS grid, with a median filter using four surrounding points. The vertical discretization of the field has been defined so as to preserve the high resolution of the Argo profilers; it is one of the major differences between the ISAS fields and the NODC climatologies (Levitus et al. 2012). A total of 152 levels have been selected between 0 and 2000 m. Two surface levels are defined at 0 and 3 m; the vertical resolution is 5 m from 5 to 100 m, 10 m from 110 to 800 m, and 20 m from 820 to 2000 m. Each level is analyzed independently.

The optimal interpolation is performed on anomalies relative to the reference field used as a first guess. The analysis modifies the first guess according to the observations on the one hand and statistical knowledge on the scales and amplitude of the anomalies on the other hand. In poorly observed areas, the solution remains close to the reference field. The covariance matrices $\mathbf{C}_{\mathrm{oo}}$ and $\mathbf{C}_{\mathrm{ao}}$ are built using the same structure function $C(dx, dy, dt)$, modeled as the sum of two Gaussian functions of time and space distances:

$$C(dx, dy, dt) = \sum_{i=1}^{2} \sigma_{Li}^2 \exp\left(\frac{dx^2}{2L_{xi}^2} + \frac{dy^2}{2L_{yi}^2} + \frac{dt^2}{2L_{ti}^2}\right), \tag{4}$$

where dx, dy, and dt are the space and time separations and L_x, L_y, and L_t the corresponding e-folding scales.

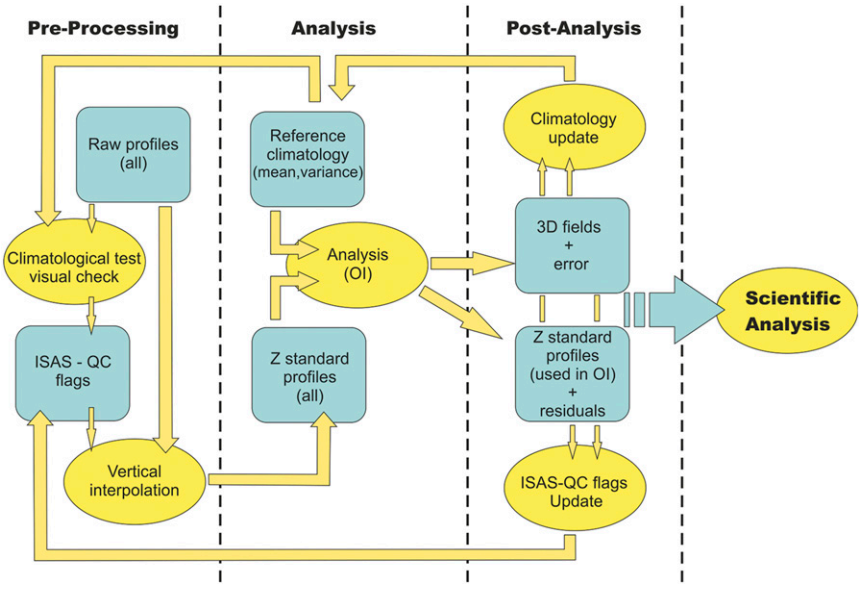

FIG. 1. ISAS processing cycle. Starting from datasets downloaded from data centers or provided by PIs, ISAS produces monthly 3D-gridded fields of temperature and salinity, qualified datasets described by residuals, and new quality-control flags and new climatologies (mean fields and variances).

The weight given to each ocean scale of variability is controlled by the variances σ^2_{Li}.

The **R** matrix that includes the measurement and the representativeness errors is assumed diagonal, which means that the errors as seen by the observing system are uncorrelated:

$$R_{ii} = \sigma^2_{\mathrm{UR}i} + \sigma^2_{\mathrm{ME}i}. \tag{5}$$

The total variance is the sum of four terms:

$$\sigma^2 = \sigma^2_{L1} + \sigma^2_{L2} + \sigma^2_{\mathrm{UR}} + \sigma^2_{\mathrm{ME}}, \tag{6}$$

where σ_{L1} and σ_{L2} are the two terms appearing in Eq. (4); σ_{UR} represents small scales unresolved by the analysis; and σ_{ME} corresponds to the measurement errors. A unique σ_{ME} profile has been computed from the measurement errors of the standard database and subtracted from the total variance to obtain the ocean variance σ_{ocean}. We express the variances associated to each scale as a function of the ocean variance by introducing normalized weights ($W_1 + W_2 + W_3 = 1$):

$$\sigma^2_{L1} = W_1\sigma^2_{\mathrm{ocean}}, \quad \sigma^2_{L2} = W_2\sigma^2_{\mathrm{ocean}}, \quad \text{and}$$
$$\sigma^2_{\mathrm{UR}} = W_3\sigma^2_{\mathrm{ocean}}. \tag{7}$$

b. *ISAS analysis: An iterative process*

The analysis can be summarized as the iterative process sketched by Fig. 1, where each cycle is decomposed in four steps.

1) INITIALIZATION

The analysis process is initiated by preparing the set of a priori statistics. The reference is provided as monthly mean fields on the analysis grid. The variance around each monthly mean is provided on the same grid. At the moment, because of the lack of data in some areas, the variance is the same for all months. The horizontal scales of the first Gaussian (L_{x1} and L_{y1}) are constant, and this term represents the limited resolution of the Argo network, if the data density increases its weight may be reduced. The horizontal scales of the second Gaussian (L_{x2} and L_{y2}) are specified at each grid point, and this term corresponds to the oceanic signal we aim to resolve. The varying covariance scales (L_{x2} and L_{y2}) are proportional to the Rossby radius associated to the first dynamical mode. They are deduced from the annual mean density profiles of the reference field that we extended to full depth using the *WOA05* climatology. The relative weights of the Gaussians (W_1 and W_2) are specified by the user. In the experiments presented here, the weight of unresolved scales (W_3), is chosen to be twice the weight of the ocean scales resolved by the analysis.

2) PREPROCESSING

Climate studies require homogenous and unbiased time series, which means that the datasets must be carefully validated, calibrated, and sometimes adjusted. In general, data centers carry on a quality control in real

time (RT) by applying widely accepted sets of criteria. The delayed-mode (DM) processing is most often performed by scientific teams and involves more subjective methodology. When dealing with global datasets, one will have to combine the various data streams and take advantage of the service provided by data centers and of the expertise of the scientific teams. ISAS analysis distinguishes two main types of datasets.

- Several data centers in the world intend to collect as many data as are available, either in real time or in delayed mode. They apply automatic quality control, sometimes complemented by more elaborated checking, and produce GADS containing all data types for the global ocean over a given period. The most current use for those datasets is data assimilation. Such datasets have the great advantage of completeness, and they allow for real-time delivery and present the data in a fashion convenient for most global synthesis tools. However, updating the dataset when the data from a particular platform have changed requires exploring the whole database.
- Many data were collected from well-identified platforms or during a specific cruise and benefited from a specific delayed-mode processing by the scientific team that collected them. These delayed-mode data are delivered by the responsible scientist as PODS and often join a thematic database. An example of such a database is the CLIVAR and Carbon Hydrographic Data Office (CCHDO) that was established during WOCE for the hydrographic data. In the case of Argo data, this mode of delivery is by far the most efficient, since the data undergo several reprocessings that are applied for all the data of a profiler at once. With the PODS it is very easy to identify which part of the dataset has been changed and needs to be reprocessed. In that case, the updating can be described as macroscopic, while it is microscopic in the GADS.

At the beginning of the project, the ISAS analysis relied entirely on GADS, but as years passed, more and more reprocessed delayed-mode PODS were available and had to be taken into account. In the current version of ISAS, for each monthly analysis, if PODS is available for a platform, all data from this platform found in the GADS are ignored. We also build our own quality-control (QC) flag files, which we attach to each POD, that allow us to reconsider the QC without modifying the original data files.

We use only the data considered as good or probably good (QC = 1 or 2 for Argo data); however, it appeared that erroneous data remained undetected. We thus perform a climatological test by comparing the profile to the reference field. When a profile shows data values more than six standard deviations away from the climatology, the full dataset from the platform (Argo float, glider, and mooring) is visually controlled, and erroneous data points are flagged as necessary. This step is important since it often happens that perfectly good sections of profiles in strong eddies or fronts fall outside of the climatic range and rejecting them automatically not only deprives the analysis of an important piece of data but prevents them from being used to build better variances.

The valid data are interpolated linearly on the 152 ISAS levels. High-resolution profiles are bin averaged. Low-resolution profiles are interpolated, and an additional interpolation error, function of the distance to the measurement levels, is added to the measurement error. Profiles with their shallowest valid measurement above 20 m are extended to the surface by simply repeating this measurement, and the measurement error on extrapolated levels is increased. For that reason, since most Argo profiles stop reporting data between 7 and 3 m, we do not recommend using the analyzed levels shallower than 10 m.

3) ANALYSIS

The analysis is performed to represent the center day of each month (day 15). The time window around the analysis date converted to Julian day j_{ana} is defined as $[j_{\text{ana}} - 41, j_{\text{ana}} + 41]$; within this time window, the weight of the data depends on the decorrelation time scales L_{ti}. The global ocean is divided into 180 analysis areas that define the grid points to be analyzed at once (Gaillard 2012). A mask is associated to each analysis area to define which data will enter the analysis. The mask is an extension of the analysis area by two covariance scales, but some parts may be excluded. This is the case, for example, near Gibraltar, to prevent using data from the Mediterranean Sea when analyzing the Atlantic Ocean area. All data with valid QC that fall within the mask and within the time window are collected to form the data vector. The analysis is carried out for all areas, and the final output is the 3D-gridded estimated field and corresponding error on the one hand, the vector of data residuals on the other hand. The monthly fields are made available for scientific studies on global ocean variability, as in, for example, von Schuckmann et al. (2009), to build climate change indicators (Mercier et al. 2015) or for process studies (Kolodziejczyk and Gaillard 2013).

4) POSTANALYSIS

The results of the analysis are also used to prepare the next iteration. The postanalysis quality control (PA-QC) is performed by screening the analyzed fields and the residuals to check the consistency with the a priori

statistics (Gaillard et al. 2009): too large an anomaly or a residual relative to the corresponding variance leads us to revise the corresponding data QC flag. A new set of a priori statistics is also prepared: the new monthly mean reference fields are obtained by averaging the corresponding gridded fields, and the new variances around the new reference state are computed on the dataset after adjusting the QC flags.

3. History of ISAS analyses

a. Globally assembled datasets used

The GADS used for ISAS are downloaded from Coriolis, the MyOcean In Situ Thematic Assembly Centre (INS TAC). In 2009, Coriolis issued the Coriolis dataset for Reanalysis, version 2.2 (CORA2.2), which we used to perform the first ISAS global analysis of the period 2002–08. Since 2009, Coriolis prepares near-real-time (NRT) monthly datasets that are made available around the 8th of each month. We downloaded the CORA and NRT GADS and performed the preprocessing climatology control. This tedious and time-consuming task appeared necessary since a number of platforms with drifting sensors or errors in data transmissions or decoding have been detected. It should also be noted that we do not use XBTs or expendable CTDs (XCTDs) to avoid problems of the vertical reference due to uncertainty in the falling rate. Another reason for excluding XBTs is to maintain homogeneity between the distribution of temperature and salinity data and be able to perform consistent computation of density. We assume that the Argo network will readily replace the XBT casts. Data located on bathymetry shallower than 15 m are excluded.

b. Platform-oriented datasets used

Since 2009, the GADS are downloaded in near–real time to produce the monthly analysis and monitor the time evolution of the temperature and salinity fields. By doing so, we do not benefit from the updates in the quality control or the delivery of delayed-mode datasets. On the other hand, retrieving new version of the global dataset as they become available would annihilate the cautious checks performed by our preprocessing, and identifying individually which profiles have been changed appeared extremely tedious. It was then decided to experiment with the use of the PODS. Three types of PODS have been selected:

- Argo floats: Two sets of Argo float data that we knew had been carefully checked by the principal investigators (PIs) were selected: 1) a set of 44 Argo floats that were deployed in the Atlantic subpolar gyre between 2002 and 2010 by the Ovide project (Mercier et al. 2015) and 2) a set of 94 Argo floats deployed in the Southern Ocean between 2004 and 2010, many of them by the GoodHope project (Rusciano et al. 2012). The corresponding PODS were downloaded from Coriolis, which acts as one of the two GDACs for the Argo network.
- Marine mammals: At the present time, salinity data collected by marine animals cannot be used in real time because the highly miniaturized inductive sensors are sensitive to pressure effects and external modifications of the magnetic field. These data should be removed from the GADS, but it is not easy to identify which version (RT or DM) appears in the GAD. Since they represent a unique set of information on the very high latitudes, it is very important to incorporate the corrected datasets in the reanalysis. A first delayed-mode dataset collected by 26 elephant seals equipped with temperature–salinity (T–S) sensors recently corrected for sensor drift (Roquet et al. 2011) were provided to us by the PIs.
- TAO/PIRATA moorings: Since January 2012, these data no longer appear in the standard NRT files (we discovered later that they were in specific NRT moorings files). We took this opportunity to test the platform-oriented processing on this dataset. The data were downloaded as PODS from the TAO data delivery website for this particular year. Although the 2012 data were not yet calibrated, they represent an important constraint in the rapidly variable upper layer of the tropical band that we did not want to lose. In future analyses, the full time series of TAO moorings, including delayed-mode calibrated data, will be retrieved as PODS.

c. Iterations leading to ISAS13 analysis

1) ISAS09 ANALYSIS

A first analysis of the period 2002–08 has been performed with the CORA2.2, selecting the raw data type. This dataset is called globally assembled dataset (GA-01) (Table 1). The reference fields were based on the *WOA05* climatology available at that time. The *WOA05* monthly fields were interpolated on the ISAS grid (the annual mean was used for the levels where no monthly field exists). To compute the covariance matrices needed for the OI, the ISAS00 standard deviation (STD) gridded fields (ISAS00-STD) were deduced from the GA-01 dataset, using as a lower bound the maximum of *WOA05* STD, and 0.06°C for temperature [or 0.015 practical salinity scale (PSS) for salinity]. The set of configuration parameters is defined as the S1 configuration in Table 2. This experiment was distributed as the

TABLE 1. Description of the datasets.

Name	Description
GA-01	CORA2.2, Coriolis reanalysis global dataset (2002–08) Raw data selected
GA-02	CORA2.2, Coriolis reanalysis global dataset (2002–08) Coriolis near-real-time global dataset (2009–11) Adjusted data selected if available
GA-03	CORA2.2, Coriolis reanalysis global dataset (2002–08) Coriolis near-real-time global dataset (2009–12) Reprocessed Coriolis near-real-time dataset (Jun–Sep 2010) Adjusted data selected if available PA-QC performed
PO-01	DM Argo Ovide (44 floats) DM Argo GoodHope (94 floats) DM elephant seals (26 sensors) DM and RT TAO 2012

ISAS09 analysis (ISAS09-ana; see the experiment summary given Table 3). This time series has been used to describe the main variability patterns diagnosed by the Argo network (von Schuckmann et al. 2009). We obtained the first ISAS climatology (ISAS09-clim) by averaging the seven years of analysis.

2) ISAS11 ANALYSIS

In 2011, a sensitivity experiment has been carried out on the period 2004–10. The years 2002 and 2003, were not considered because of the strong undersampling of the Southern Ocean. The dataset named GA-02 used results from the combination of the CORA2.2 dataset with the NRT dataset for the years 2009 and 2010. The adjusted data types were selected for all files. The first experiment (TEST11-a) was performed with the same reference and configuration as the ISAS09 experiment. For the second experiment (TEST11-b), the ISAS09-clim was used as reference, and the a priori variances ISAS09-STD were computed with the same methodology used to produce ISAS00-STD, using the GA-02 dataset referenced to ISAS09-clim. The configuration parameters have been adjusted to produce the analysis distributed as ISAS11: more weight was given to the varying L_2 covariance scale, and the time scale was increased from 21 to 30 days (S2 configuration).

3) ISAS13 ANALYSIS

The latest analyses were performed over the period 2002–12. Meanwhile, the version of ISAS tool has evolved from version 5 to 6, the major changes being that the L_2 covariance scales can now be specified differently for the x and y directions. To minimize the changes with respect to previous versions, this possibility is used only to increase the zonal scales in the tropical band by raising the upper bound to 600 km in the zonal (x) direction. The new configuration, named S3, is described in Table 1. The reference climatology for these experiments is ISAS11-clim, the mean of ISAS11 analysis (ISAS11-ana).

The first experiment (TEST13-a) uses the GA-02 dataset, extended to 2012. The distributed ISAS13 analysis (ISAS13-ana) is based on a cleaner global dataset (GA-03) that benefited from the PA-QC and the data recovery of a few months of 2010. Moreover, a first attempt to include identified platform-oriented datasets (PO-01) has been performed. The data distribution in space is summarized in the map shown Fig. 2. The improvement in the sampling attributed to Argo is clearly seen when comparing the total number of salinity data points per square degree of area at 1500 m to its *WOA05* equivalent: in the Southern Ocean (around 40°S), for example, where *WOA05* had between 5 and 30 data points, we now have between 60 and 150 data points. The *WOA05* climatology will be considered here as a reference for the pre-Argo period.

Special care has been taken to improve the a priori variances by applying the following methodology: A monthly variance is computed at each grid point as the mean square anomaly relative to the local monthly climatology for all data within a square of size 10 grid cells (5° at the equator). The annual mean standard deviation (ISAS11-STD) is the square root of the mean monthly variances. To take into account that some areas remain undersampled (the Southern Ocean, in particular) and that some erroneous data may remain in the dataset, we impose an upper and a lower bound, and for data void areas a default value is proposed. These values were obtained as follows: At each level, we computed the

TABLE 2. Description of the configurations. The W_i^* provided are not normalized; the normalization ($\sum W_i = 1$) is performed later by ISAS.

Configuration name	ISAS version	$L_{t1,2}$ (days)	$L_{x,y1}$ (km)	$L_{x,y2}$ (km)	W_i^*, $i = 1, 2, 3$
S1	5	21	300	x, $1.5dy < 2\pi R < 300$ km	1, 1, 4
			300	y, $1.5dy < 2\pi R < 300$ km	
S2	5	30	300	x, $1.5dy < 2\pi R < 300$ km	1, 2, 6
			300	y, $1.5dy < 2\pi R < 300$ km	
S3	6	30	300	x, $1.5dy < 2\pi R < 300$ km	1, 2, 6
			300	y, $1.5dy < 2\pi R < 300$ km	

TABLE 3. Description of the experiments. The rightmost column gives the name under which this analysis is distributed.

Experiment name, period	Configuration	Reference climatology	GADS	PODS	Analysis or climatology name, period
ISAS09, 2002–08	S1	*WOA05* climatology ISAS00-STD	GA-01	none	ISAS09-ana, 2002–08 ISAS09-clim, 2002–08
TEST11-a, 2004–10	S1	*WOA05* climatology ISAS00-STD	GA-02	none	
TEST11-b, 2004–10	S1	ISAS09-clim ISAS09-STD	GA-02	none	
ISAS11, 2004–10	S2	ISAS09-clim ISAS09-STD	GA-02	none	ISAS11-ana, 2004–10 ISAS11-clim, 2004–10
TEST13-a, 2002–11	S3	ISAS11-clim ISAS11-STD	GA-02	none	
ISAS13, 2002–12	S3	ISAS11-clim ISAS11-STD	GA-03	PO-01	ISAS13-ana, 2002–12 ISAS13-clim, 2004–12

distribution of STD with the lower bound defined as the value of the first 0.6th percentile, and the upper bound is the value of the 99.9th percentile from 0 to 20 m and of the 99.5th percentile below 20 m. The default value is the most probable value. An exponential is fitted through the lower bound and default value vertical profiles; for the maximum a smooth profile was obtained by applying a linear filter on the vertical profile of maximum. Finally a horizontal smoothing is performed as follows: at grid points where the number of data points is too small, the value is replaced by the mean of the value of the well-estimated points within a four-gridpoint square cell (Gaillard 2012).

A similar exercise has been performed after the ISAS13 analysis to compute ISAS13-clim (the mean fields) and ISAS13-STD. The standard deviations (shown in Fig. 3) have evolved from ISAS00-STD to ISAS13-STD. The first important change occurs from ISAS00-STD to ISAS09-STD. The ISAS00-STD were computed relative to a mean state that does not correspond to the period of the dataset (we used the *WOAO5* mean) and thus include the bias due to the long-term trend, which tends to increase the variance. On the other hand, the fields were computed with a reduced dataset, in particular salinity in the Southern Ocean, which leads them to underestimate the variance and explains the very low values seen in the three ocean basins (Fig. 3). In the Southern Hemisphere, the variances (or STDs) show a continuous increase from ISAS00 to ISAS13. This is particularly obvious for salinity and results from the better sampling due to the Argo network. The high salinity variances noted in the ISAS09 and ISAS11 datasets south of 50°S are as a result of the erroneous data from uncalibrated sensors carried by the marine mammals that were not detected at that time. They have been replaced by the calibrated data in ISAS13. The ISAS13-STD fields, which include a more complete dataset, better represent the variability of the ocean (Fig. 4). They should allow for an improved estimate of the monthly fields and corresponding error when used as a priori statistics for the next ISAS reanalysis.

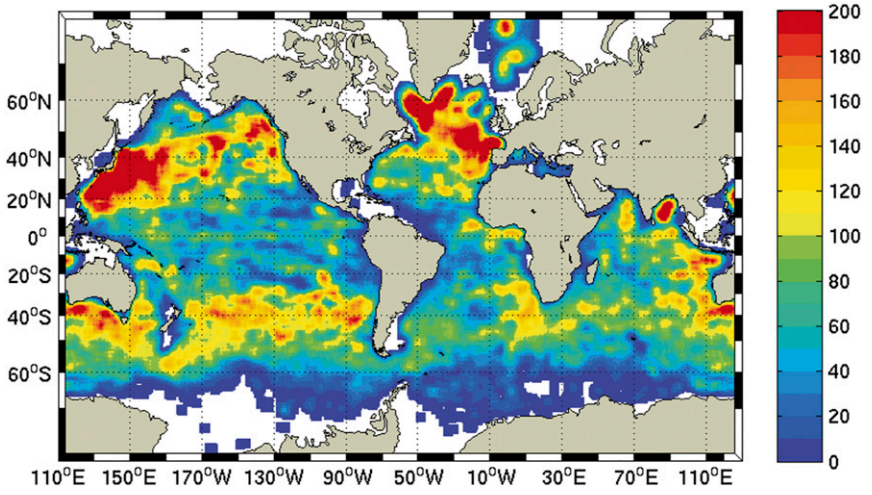

FIG. 2. Total number of salinity data points per square degree of area at 1500 m for the period 2002–12.

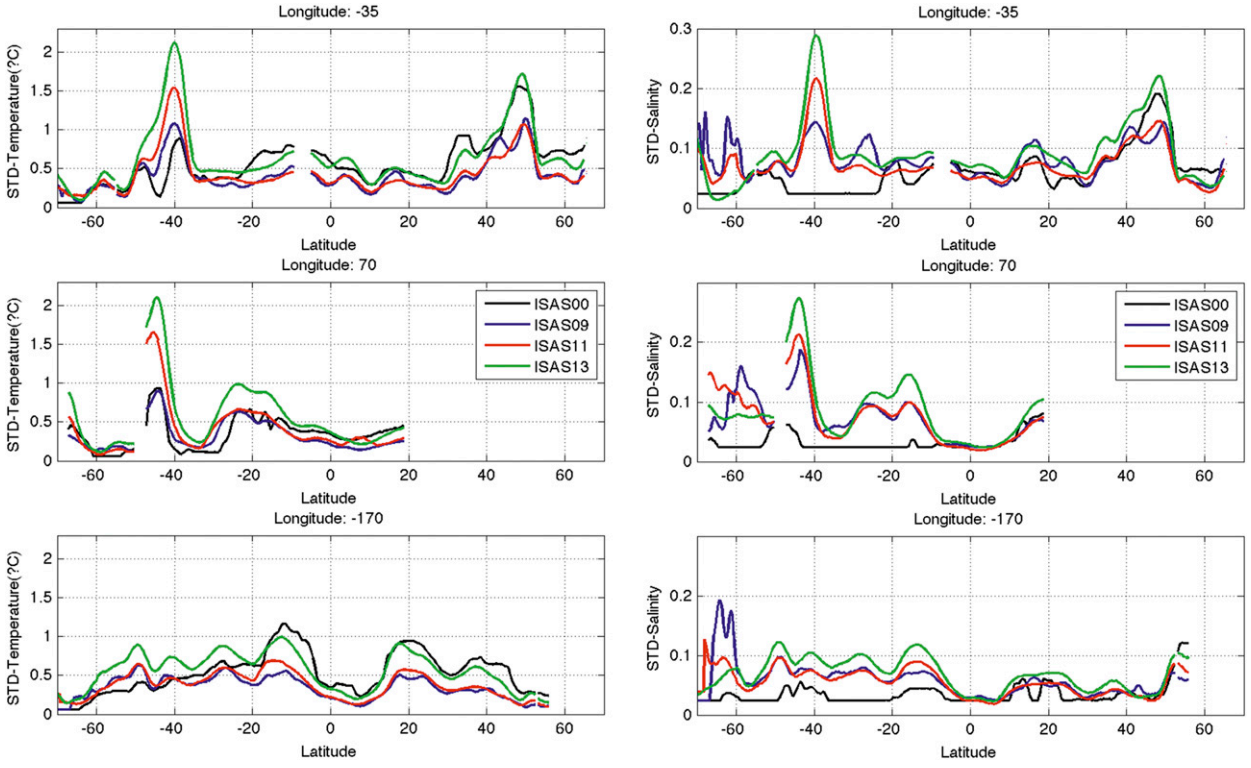

FIG. 3. Standard deviation of (left) temperature and (right) salinity in the reference climatologies used to produce the ISAS analysis presented in this paper. The standard deviation at 300-m depth is presented along three longitudes selected in the (top) Atlantic (35°W), (middle) Indian (70°E), and (bottom) Pacific (170°W) Oceans.

d. Summary of the advances of the new ISAS13 analysis

The major changes in the ISAS13 analysis relative to the previous analysis can be attributed to the following.

- Better data processing: More recent Argo DM datasets delivered by PIs appeared in the Coriolis dataset. Some Argo floats profiles have been detected as bad either by the preprocessing eye screening or postprocessing consistency tests exposed in the previous section. We used the delayed-mode datasets from elephant seals for ISAS13, while real-time data were used in previous analysis.
- Better a priori statistics: The ISAS11 climatology (mean and variance) used for ISAS13 better represents the mean state of the ocean than the previous versions, in particular for salinity and the Southern Ocean, which were previously undersampled. The L_2 covariance scales proportional to the Rossby radius are given more weight in ISAS11 and ISAS13. They are allowed to reach 600 km in the zonal direction in ISAS13. This choice was made following Delcroix et al. (2011). The extended zonal scales in the tropical band allow for a better use of the TAO moorings in particular.

Basically, the algorithm has not changed since the ISAS09 analysis. Up to now, most of the problem has arisen from the data sampling, erroneous data, or sensor drift, therefore, we have focused our efforts on these aspects. There is room for improvement to better represent the marginal seas, coastal areas, and frontal zones. In coastal areas, the covariances are reduced through the decrease of the Rossby radius, but they remain isotropic. In order to take into account that scales are larger along the bathymetry than across, a penalizing f/H term, where f is the Coriolis parameter and H is the ocean depth, could be introduced in the covariance function. The question of analyzing all levels independently may also produce unrealistic discontinuities; the method proposed by Chang and Shin (2014) could be tested in a local configuration (one of our areas, for example).

4. Robustness of global heat content and steric height

It appears that global OHC and global SH are the synthetic quantities most commonly used as a measure of global change. OHC expresses the temperature changes, while SH results from the combined effect of temperature

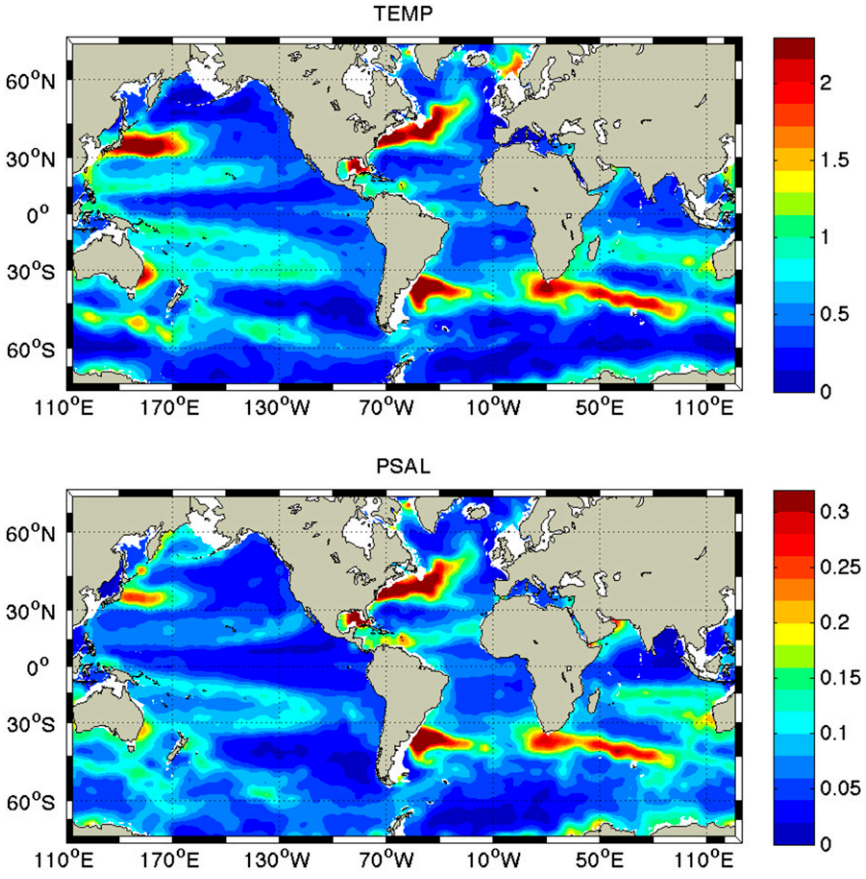

FIG. 4. ISAS13-STD at 300-m depth for (top) temperature (°C) and (bottom) salinity (PSS). The STDs represent the temperature and salinity variability captured by the 2004–12 dataset, relative to the ISAS13-clim, which represents the large-scale mean over this period. Most of the variability is associated with the strong current systems.

and salinity changes on seawater density. It is still difficult to obtain true global quantities with analysis based on in situ observation alone: the very high latitudes and the deep oceans are too poorly observed for attempting any monthly estimate there. The integration of OHC and SH have been restricted here to the domain extending from 60°S to 60°N and the vertical range 0–1500 m, selected for being acceptably sampled over most of the 2002–12 period.

The time series of global OHC and SH computed for all the experiments are presented in Fig. 5 as anomalies relative to the *WOA05* climatology, which thus corresponds to the zero line of the graphs. The seasonal signal has been removed from the time series. The ISAS09 OHC and SH time series show intraseasonal-to-interannual variability overlying a rapid increase over the six years of the period analyzed. Using the adjusted data type (TEST11-a) leads to higher values of OHC ($+0.8 \times 10^{22}$ J) and SH (+0.1 cm) in 2004–06 and slightly lower values of OHC and SH in 2007–08 leading to reduced trends. Switching to the first Argo-based ISAS09 climatology (TEST11-b and ISAS11 experiments, shown as blue curves in Fig. 5) introduces a major change in the OHC and SH time series in 2004 with values of OHC 3×10^{22} J higher with the new reference (the sensitivity experiments based on ISAS09 were not conducted on the 2002/03 period). The difference between the ISAS09- and *WOA05*-referenced experiment decreases to about 1×10^{22} J by the end of 2006. Despite these important differences at the beginning of the period, intraseasonal-to-interannual variability is similar in all experiments. The differences are easily explained by the methodology: the analyzed field is a modification of the reference field deduced from the observations and weighted by the a priori variances and covariances. When and where the observations are missing, the solution remains close to the reference represented by the zero line for the *WOA05*-referenced experiments and by an OHC value close to 4×10^{22} J yr^{-1} in the

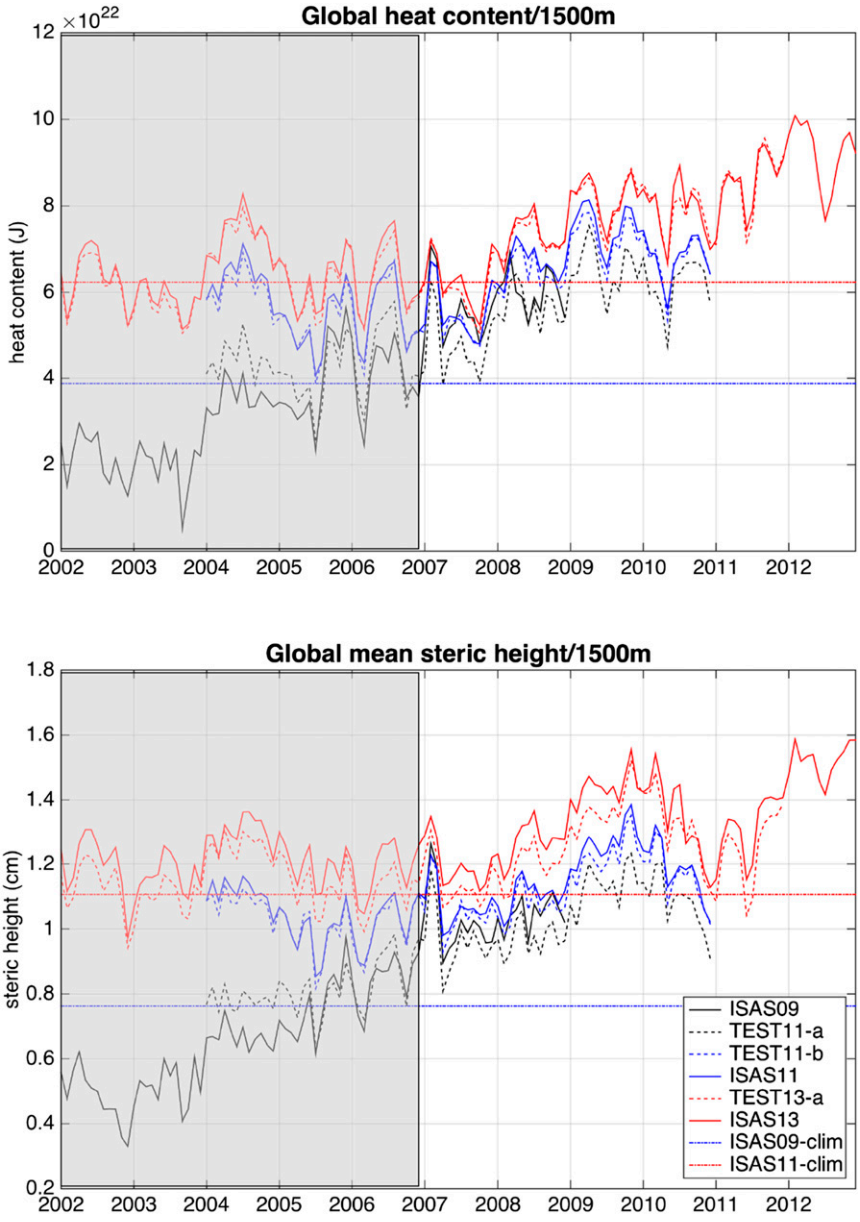

FIG. 5. (top) Global OHC integrated from 0 to 1500 m and (bottom) global SH relative to 1500 m in the different experiments: the experiments using *WOA05* as reference climatology (black), the experiments using ISAS09-clim (blue), and the experiments using ISAS11-clim (red). The global quantities are computed relative to their *WOA05* equivalent; integration is performed from 60°S to 60°N. The period during which the estimate is not reliable because of insufficient sampling of the Southern Hemisphere, in particular, has been shaded in gray.

ISAS09-referenced experiments. The last series of analysis (TEST13-a and ISAS13, shown as red curves in Fig. 5) performed over the period 2002–12 and referenced to the ISAS11 climatology show OHC values shifted by 1×10^{22} J relative to the previous set of experiments; little differences are noted when the delayed-mode datasets, which are still a modest contribution, are included. Changes introduced by the new climatology are more important in the SH series, indicating that the salinity information carried by the 2004–10 ISAS11 reference climatology (that benefits from the fully developed Argo network) is really a new contribution with respect to the image reported by the *WOAO5* climatology. The difference is even stronger when using the delayed-mode data because the major changes between real-time and delayed-mode processing apply to salinity, which influences the SH.

The least squares method used here biases the estimator toward the reference state, and any anomaly with respect to the mean state is treated as random, which leads it to underestimate the anomalies. Better results could be obtained by using the last analyzed field as a reference to compute the next analysis. This process, known as Kalman filtering, requires computing the full error matrix (not only the diagonal terms as in OI), which considerably increases the computational cost. Moreover, this will overweight the impact of a bad profiler. We thus made the choice of remaining simple, leaving the full assimilation process to operational models (such as Mercator). The present work only pretends to offer an in situ reference. However, a different strategy will have to be designed when dealing with longer time series (several decades), where the long-term trend represents a significant part of the variance.

The analysis of the results of this sensitivity experiment raises two questions about the gridded fields produced with ISAS: 1) Are the different results compatible? 2) When can we start using the gridded fields with reasonable confidence? ISAS relies on a statistical methodology that provides error estimates at each grid point. It is thus possible to obtain an error estimate on the integrated quantities by using this point estimate and taking into account the correlation scales of the results. The basic principles are explained in von Schuckmann et al. (2009). According to this computation, the estimated error remains close to 0.4×10^{22} J for the 2002–08 period in the ISAS09 analysis. The same error decreases from 0.51×10^{22} J in 2002 to 0.36×10^{22} J in 2012 in the ISAS13 analysis. It thus appears that the results of the different experiments are compatible within error bars only after 2006 for OHC. This is somehow embarrassing but not really surprising. The incompatibility noted during the first years indicates that at least one hypothesis on which the statistical method relies is not verified. The most likely candidate is the a priori variance. In areas where little is known about the variable (temperature or salinity), the variance is strongly underestimated. This leads to underestimates of the anomaly but also of the absolute error. In data-void areas, even a 99% error may lead to an unrealistically small error if the variance is too small. The full answer to the first question is thus: the results are not compatible within error bars because error bars are underestimated in areas that were poorly sampled by the database used to compute the a priori variances. And this is particularly true for the ISAS09 experiment. Although the estimate of the anomaly cannot be improved where the ocean has not been sampled, the estimate of the corresponding error can be significantly improved with better a priori variances. It is thus important to reevaluate the variances each time the dataset increases and define lower bounds for the less-sampled areas. This point is an important part of the iterative strategy for the ISAS reanalysis.

The answer to the second question is more intricate. Clearly, global trends cannot be deduced from the present analysis since only six years (2007–12) are estimated with reasonable error bars, which does not allow us to resolve the decadal variability; however, some areas have been observed better in the early stages of Argo. When considering separately the southern, tropical, and northern latitude bands, robustness of OHC appears to behave differently (Fig. 6). North of 30°N, where the Argo network was first deployed, the different analyses are in full agreement since 2007 but already give compatible results before (the same is true for SH). In the Southern Ocean (south of 30°S), the OHC estimates agree well after 2007 and marginally in 2005/06. Large discrepancies are observed in 2002–04, when the estimates tend to stick to their reference field for dramatic lack of data and insufficient a priori variance. In the tropical ocean, we note a nearly constant bias between ISAS11 and ISAS13 estimates: the same bias that was observed in the global curves of Fig. 5. Three factors contribute to obtain estimates of a stronger anomaly in ISAS13: 1) the ISAS11 climatology used as reference for the ISAS13 analysis has captured changes relative to *WOA05* that were still underestimated in the ISAS09 climatology, so the analysis has a better starting point; 2) the corresponding variances have increased, and the estimate will move away from the reference more easily; and 3) the larger horizontal covariance scales in the zonal direction allowed in the tropical band lead to a better use of the data at these latitudes in the ISAS13 analysis.

5. The ISAS13 analysis and climatology

a. The ISAS13 decadal mean

As noticed in the previous section, the length of the series does not allow for reliable estimates of long-term trend, not even decadal variability within the observed period. However, it is also clear that the mean state of the ocean during 2002–12 is different from the mean state of the period represented by *WOA05*. The ISAS13 climatology representative of the period that we assume to be reasonably sampled with Argo has been computed by taking averages over the 2004–12 period (9 yr). The corresponding mean anomalies of ocean heat content (0–1500 m) and steric height (surface relative to 1500 m) relative to *WOA05* long-term mean have been deduced from the ISAS13 climatology (Fig. 7). Large-scale features

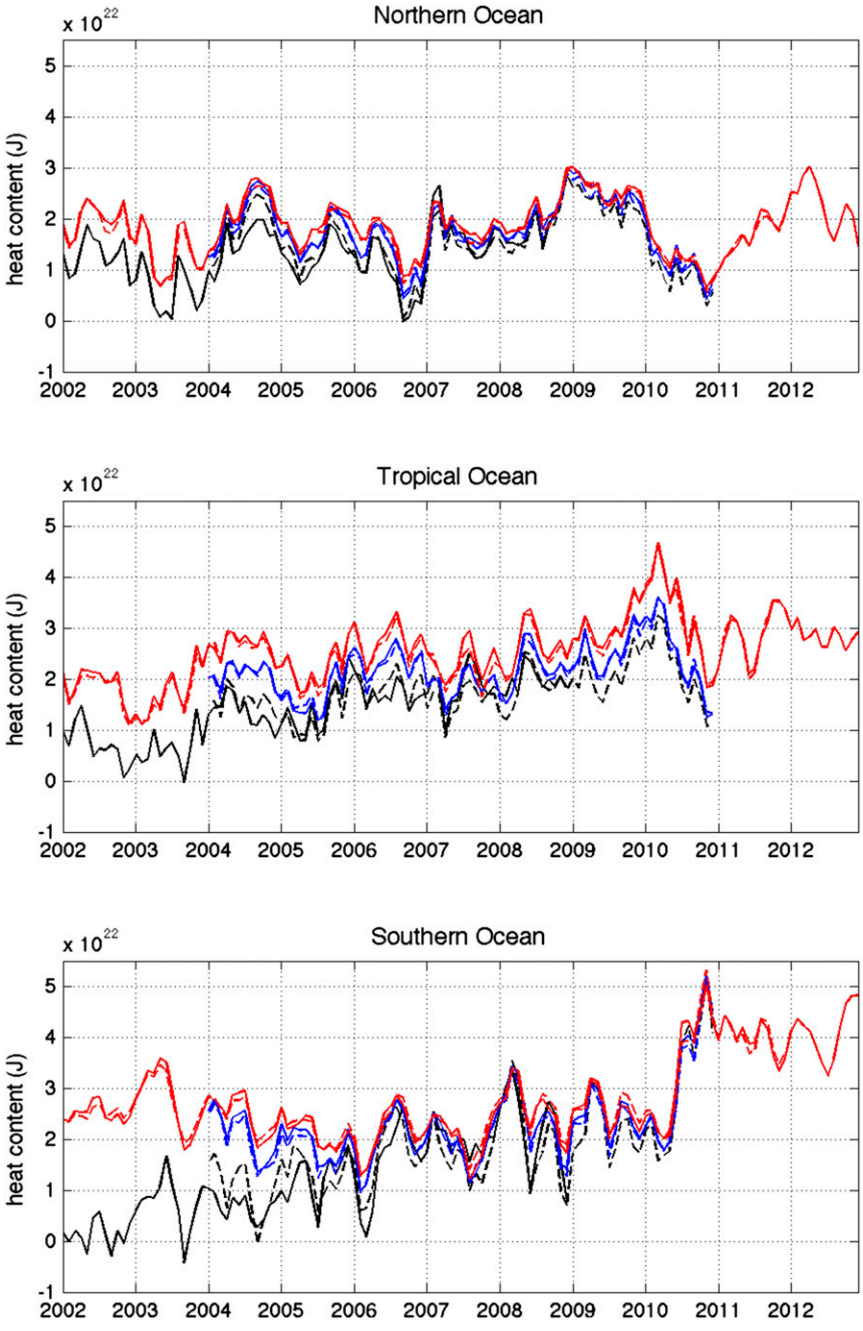

FIG. 6. OHC integrated from 0 to 1500 m and over different latitude ranges. (top) northern ocean (30°–60°N), (middle) tropical ocean (30°S–30°N), and (bottom) the Southern Ocean (60°–30°S). The colors used for the different experiments are as in Fig. 5.

already noticed by Roemmich and Gilson (2009) are confirmed here: The Atlantic Ocean appears warmer, particularly in the Irminger and Labrador Seas, including the Southern Ocean. The spatial structure of the steric height anomalies show similarities with those observed in the heat content, but the amplitude of the change is the largest in the western Pacific, while the strong northern North Atlantic heat anomaly is, in part, salinity compensated. Lee and McPhaden (2008) attributed the steric height change to a change of the circulation forced by a change in the wind stress; in particular, they noted a strong positive trend in the western Pacific from 1993 to 2000 that tended to reverse from 2000 to 2006.

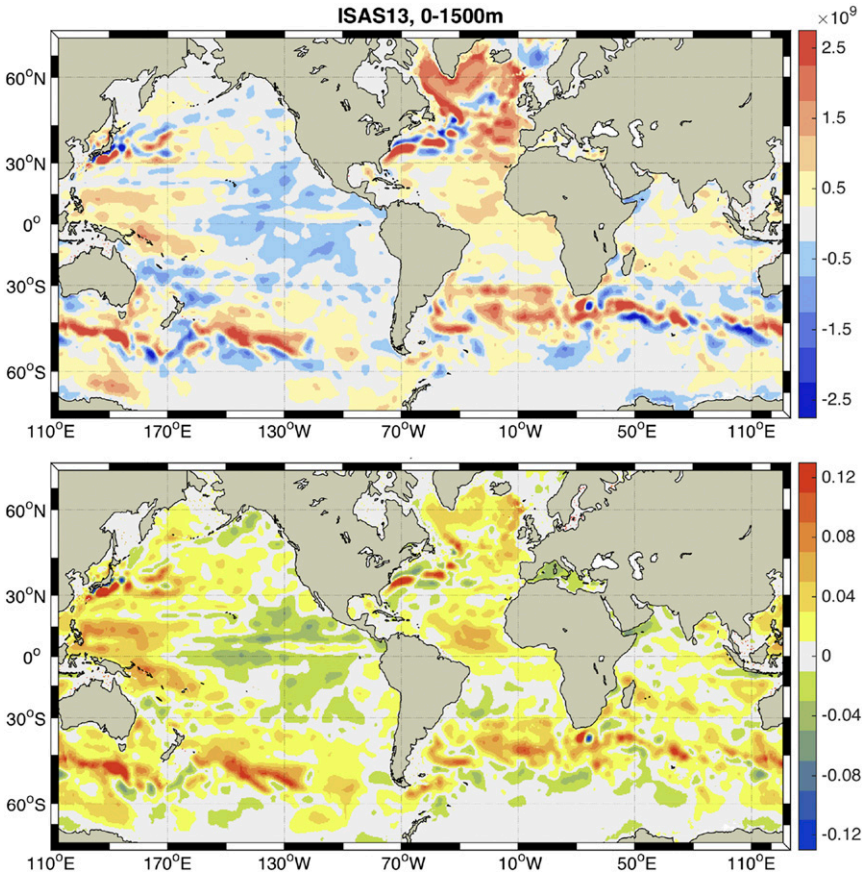

FIG. 7. ISAS13-clim (2004–12) shown as anomaly relative to the long-term reference represented by *WOA05*. (top) Ocean heat content from 0 to 1500 m (J m^{-2}) and (bottom) SH relative to 1500 m (m).

If we divide the ocean into a layer of light water that strongly interacts with the atmosphere, defined by potential density anomaly lower than 26.5 kg m^{-3} [here we use the same definition as Zilberman et al. (2014)], and a layer that corresponds to the major types of intermediate waters, with potential density anomaly in the range 26.5–27.6 kg m^{-3}, we note that changes in the surface layer concerns all oceans with similar intensity (Fig. 8). The Atlantic light waters are generally warmer and saltier than the reference climatology. In the Pacific, light waters are warmer in the west and cooler in the east. In this basin, the structures of the salinity anomalies are more complex: in particular, the large area of freshening observed along the western boundary explains the increase in steric height noted in Fig. 7.

The vertical penetration of the temperature and salinity changes differs considerably from one ocean to the other (Fig. 9). Temperature and salinity increase penetrates deeply in the North Atlantic. At opposite latitudes, a freshening change initiated around 60°S seems to spread following the path of Antarctic Intermediate Waters. The intermediate waters are warmer and saltier in the North Atlantic, except for a cold and fresh anomaly in the very center of the subpolar gyre. The changes result from a combined effect of the upper Labrador Sea Water and Mediterranean Outflow Water. The western Mediterranean Sea water has been warming and saltening continuously during the second half of the twentieth century (Zunino et al. 2009). The change in the Labrador Sea Water is more likely related to decadal variability and corresponds to a warm period observed during 1995–2006 (Sarafanov et al. 2009), associated with a phase of negative North Atlantic Oscillation (Desbruyères et al. 2013; Mercier et al. 2015). The freshening of the Antarctic Intermediate Water is seen over the whole Southern Hemisphere south of 40°S, except on the rim of the Antarctic continent, where a salty anomaly has developed. The corresponding temperature changes are not directly correlated with this broad salinity signal. The freshening of surface waters in the Southern

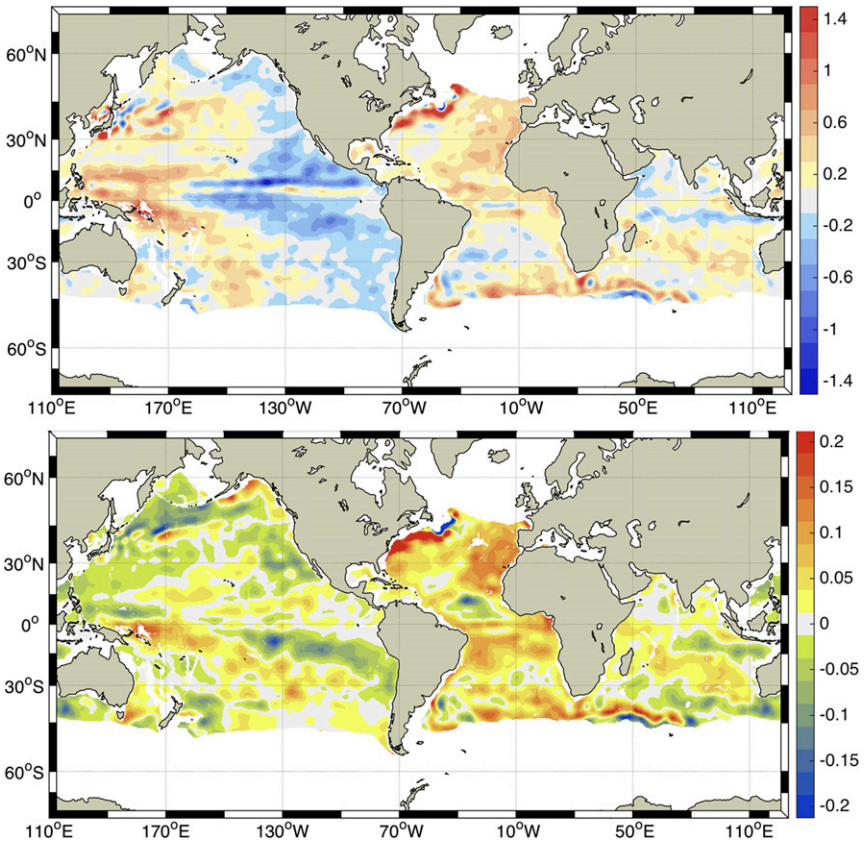

FIG. 8. (top) Temperature (°C) and (bottom) salinity (PSS) anomalies of ISAS13-clim relative to *WOA05* averaged over the light water layer ($\sigma_0 < 26.5\,\mathrm{kg\,m^{-3}}$).

Ocean has been documented by Morrow and Kestenare (2014), who relate it to the wind forcing for waters located north of the Subantarctic Front and to sea ice coverage for waters located in the Antarctic zone.

b. *Interannual variability*

Roemmich and Gilson (2011) had noticed already that El Niño–Southern Oscillation (ENSO) strongly modulates the global mean 0–500-m heat content anomaly and observed that the ocean loses heat during El Niño and gains heat during La Niña. The time series of global OHC over the 0–1500-m layer obtained with ISAS13 for the 2005–12 period confirms these findings. The time series of the global OHC change shown Fig. 10 appears anticorrelated (correlation coefficient of −0.42) with the time series of the oceanic Niño index (ONI) time series (defined as an average of sea surface temperature anomaly over the Niño-3.4 region). Note that the time series were detrended and filtered by applying a low-pass, third-order Butterworth filter with 12-month cutoff. It should be noted, however, that for the two ENSO events captured by the series: El Niño 2006/07 and El Niño 2009/10, the heat loss is moderate, while we observe a clear heat gain during the following strong La Niña (Fig. 10).

The two ENSO events are detected also in the detrended and filtered SH anomalies (Fig. 10), with an increase of SH during El Niño (2006 and 2009) and a decrease during La Niña (2007 and 2010). The global mean sea level (GMSL) distributed by AVISO have been filtered in the same way, and time series show similar anomalies associated with these two ENSO events but with stronger amplitude (correlation coefficient of 0.75). SH expresses the volume change resulting from a density change, while GMSL represents the total volume change that also includes the change of mass. Cazenave et al. (2012) studied in detail the 1997/98 El Niño and observed a strong GMSL positive anomaly that they attributed to a water mass excess in the Pacific (0°–25°N) due to a positive inflow/outflow. We show here that a steric component with minor amplitude also exists. It is also interesting to note that the steric component explains nearly one-third of the SSH decrease observed during the La Niña 2007, a decrease that could not be explained by the landmass

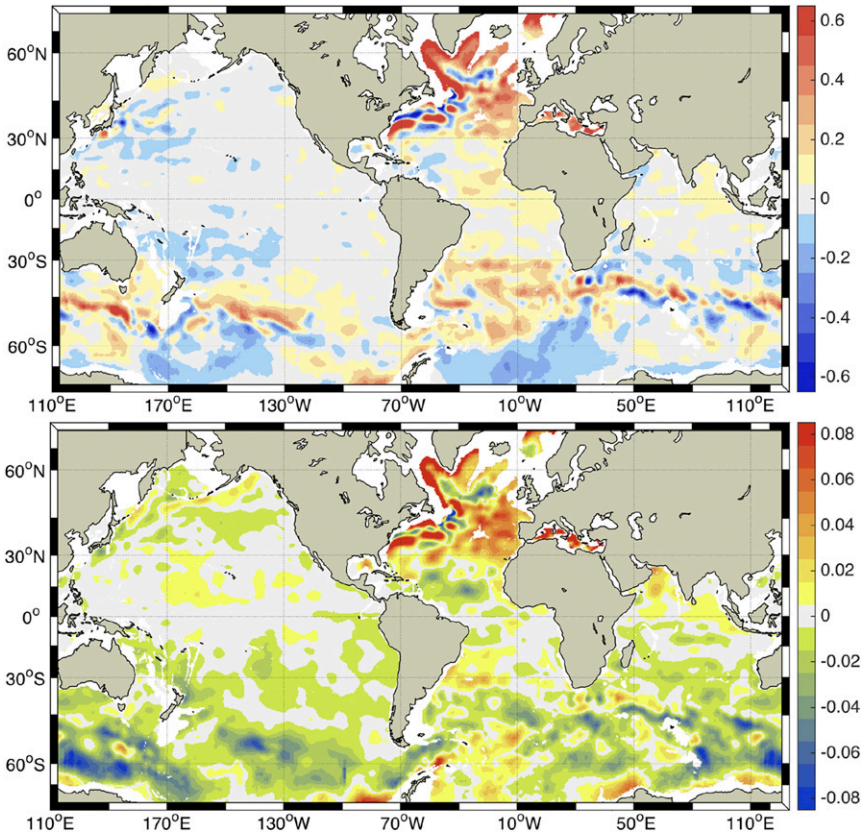

FIG. 9. As in Fig. 8, but for the intermediate waters layer ($26.5 < \sigma_0 < 27.6\,\mathrm{kg\,m^{-3}}$).

storage [see Meyssignac and Cazenave (2012, their Fig. 7)].

The 2009/10 ENSO event is particularly interesting. Two types of El Niño events are conventionally identified: the central Pacific (CP, or warm pool) type and the eastern Pacific (EP, or cold tongue) type. Yu and Kim (2013) classified the ENSO events in the period 1870–2010 and found that the two most significant recent events were the strong 1997/98 EP type and the 2009/10 CP type El Niño events. Kim et al. (2011) pointed out the particularly fast transition from El Niño to La Niña at the end of 2009. We observe (Fig. 6) a strong warming in the tropical band during 2009 that peaks at the beginning of 2010, followed by a more intense cooling until the end of 2010. As soon as the tropical band started to cool, the southern latitude gained heat extremely fast and has kept this high level of heat content since then. Examining in more detail the temperature anomalies (they are shown in Fig. 11, relative to the ISAS13-clim) after the 2009/10 ENSO, we observe in 2011 a large warming area at 10 and 300 m in the South Pacific and Indian Ocean. In 2012, the anomaly has disappeared from the surface but persists at 300 m. The same scenario was observed in the study conducted in the reanalysis for the Ocean Reanalysis Sytem 4 (ORAS4)by Balmaseda et al. (2013, their Fig. 3). Following the huge 1997/98 El Niño, OHC dropped in the tropics, particularly in the Pacific and recovers after 1–2 yr, while it rose swiftly in the Southern Ocean.

6. Summary and conclusions

The global gridded fields of temperature and salinity based on in situ measurement have been produced for the 2002–12 period covered by Argo with the analysis tool ISAS-V6. The combination of platform-oriented datasets obtained in delayed mode with the globally assembled datasets provided by the datacenter is proven to be efficient to take into account the most up-to-date datasets. The preprocessing quality control and the postanalysis validation based on residual analysis are confirmed as a reliable method to detect outliers and sensor drift. This methodology will be generalized in the future analyses.

The statistical method (OI) used in ISAS combines the observations and associated errors with statistical information to propose an estimate of the temperature

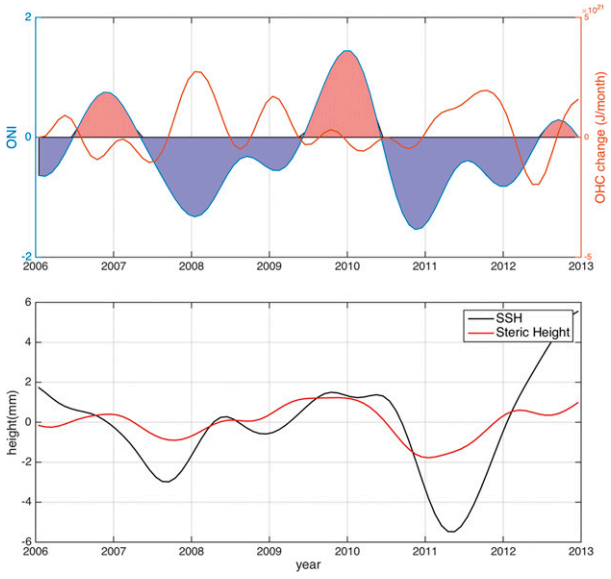

FIG. 10. (top) Detrended time series of OHC change estimated from ISAS13 analysis (red) overlaid on the ONI. (bottom) Detrended time series of SH from ISAS13 analysis (red) and AVISO sea surface height (SSH, or GMSL) (black). All series have been low-pass filtered (12-month cutoff).

and salinity fields. The sensitivity tests performed show the importance of the a priori statistics, in particular the reference field and the corresponding variances, to obtain a good estimate of the field and a correct evaluation of the absolute error. Unfortunately, before the Argo network was fully deployed, the statistics were poorly known in the least-sampled areas, such as the Southern Ocean. In those areas, the mean state represents a particular situation or is excessively smoothed, and the variance is usually strongly underestimated, but in a few cases of erroneous data, it may also be artificially increased. As a consequence, in the data-void areas, the temperature and salinity fields remain biased toward a reference that may not represent the mean state, and in the areas where the variances are underestimated, even though new data exist, they are not taken into account with the correct weight, and the errors are largely underestimated. For that reason, we propose the iterative approach that relies on updating the mean state and variances at the end of the analysis and later uses them for the next analysis, which will thus be based on a longer and better-qualified dataset. The statistics (mean and variance) will be considered as correct only when convergence is reached; then the a priori statistics will be in agreement with the field that we intend to reconstruct, and the error estimate will be reliable.

In the series of analysis proposed here, ISAS13 is a clear improvement over the previous versions, ISAS09 and ISAS11. It covers the longest time period; the dataset makes better use of the delayed-mode datasets, which makes a difference on the quantities related to salinity, such as the steric height. The reference state and the variances deduced from the ISAS11 analysis are better defined in the Southern Ocean. However, convergence of the variance has not been reached yet, and the statistical errors provided by the OI may remain underestimated.

It appears that the ocean north of 30°N is sufficiently sampled since 2002 to deduce reliable estimates of integral quantities and corresponding errors. This is not the case for the Southern Ocean south of 30°S where the sampling is too sparse before 2005/06. Moreover, in this area, the a priori variances are underestimated, which leads to lessen both the estimate of the ocean field and of the statistical error. The new statistics deduced from the ISAS13 analysis will provide an improved set of a priori statistics for the next reanalysis and allow for a better estimate of the error bars. Additional progress could also be made by providing a better description of the covariance scales based on the extended dataset that has been assembled, complemented by information from high-resolution model output. In coastal areas or near strong bathymetry, alongshore and cross-shore scales could be distinguished by introducing a term f/H in the structure function.

Global estimates are reliable only since 2006; consequently, the time series of global quantities are still too short for estimating long-term trends. However, the mean state of the 2004–12 period has been established (although it is biased toward the 2007–12 period in the Southern Ocean). The main features of the state of the ocean during that period are obtained by comparison with the long-term mean represented by *WOA05* climatology (considered as the pre-Argo period). We observed a positive anomaly of heat content over the North Atlantic and in the area influenced by the circumpolar current and a modification of the circulation in the western Pacific. The two main intermediate waters of the North Atlantic: the upper Labrador Sea Water and the Mediterranean Outflow Water are now warmer and saltier. In the Southern Ocean, the Antarctic Intermediate Water is fresher.

Interannual variability of the global quantities during the 2006–12 period is dominated by ENSO that produces global warming or cooling depending on the sign of ONI. The strong and unusual ENSO event of 2009/10 (that continued in 2011) can be followed at global scale and at all depths in the 3D-gridded fields, and a connection with the Southern Ocean is suspected. The two ENSO events observed at the end of the period may have strongly influenced the 2004–12 mean heat content anomaly of the upper layer in the tropics and in the Southern Ocean.

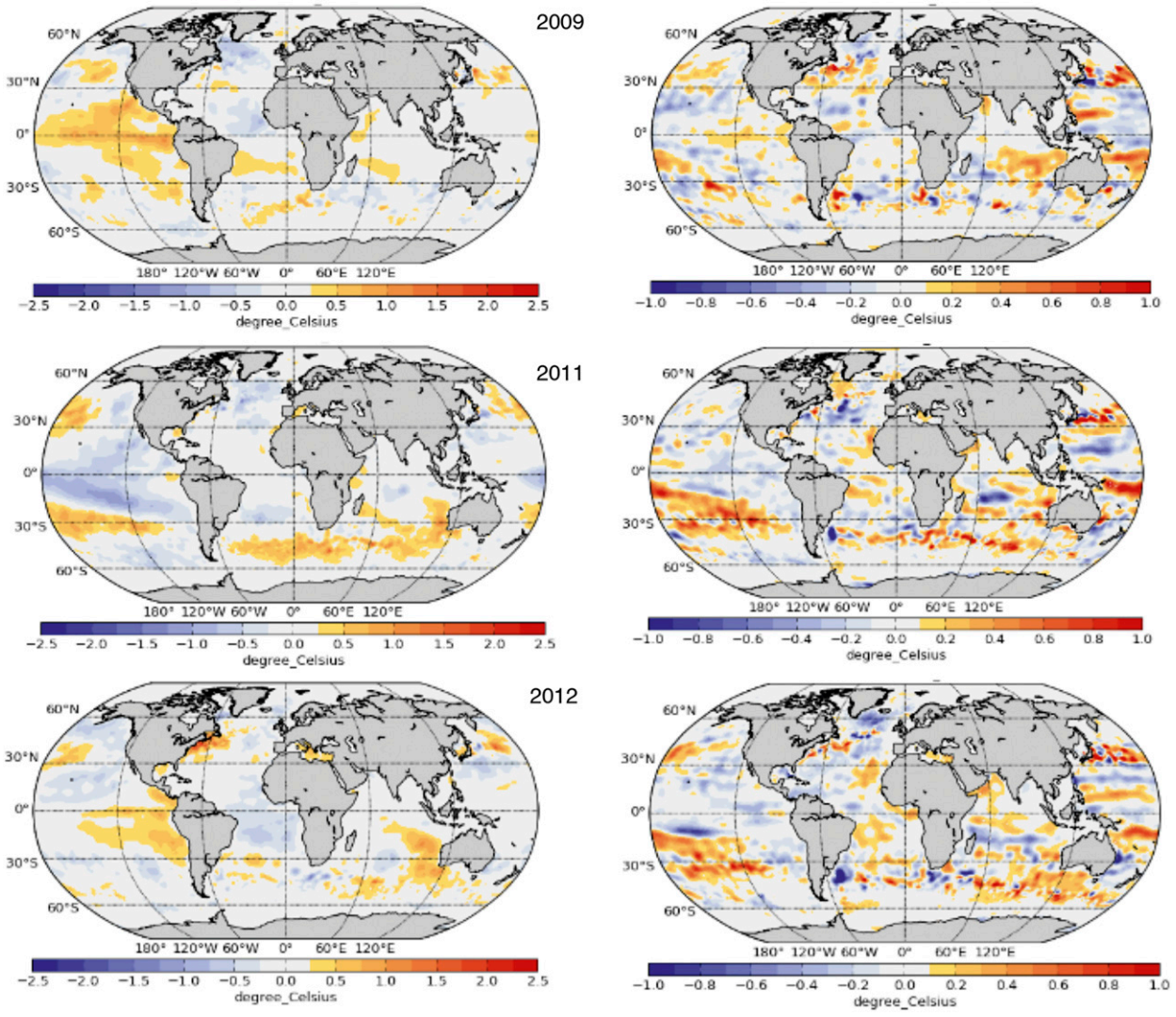

FIG. 11. ISAS13 annual mean temperature anomalies (°C) from the beginning (2009) and after (2011 and 2012) the 2009/10 ENSO at (left) 10 and (right) 300 m. The anomalies are shown relative to the ISAS13-clim.

Acknowledgments. The work presented here was funded by Ifremer program ''Ocean et Climat,'' INSU program LEFE, and CNES program TOSCA. It is mainly based on the Argo dataset and thus benefited from the strong involvement of scientists and data managers in the floats deployment and in the data validation and distribution. Remarks by the reviewers greatly helped to improve the manuscript.

REFERENCES

Balmaseda, M. A., K. E. Trenberth, and E. Kaellen, 2013: Distinctive climate signals in reanalysis of global ocean heat content. *Geophys. Res. Lett.*, **40**, 1754–1759, doi:10.1002/grl.50382.

——, and Coauthors, 2015: The Ocean Reanalyses Intercomparison Project (ORA-IP). *J. Oper. Oceanogr.*, **8** (Suppl.), S80–S97, doi:10.1080/1755876X.2015.1022329.

Bretherton, F., R. Davis, and C. Fandry, 1976: Technique for objective analysis and design of oceanographic experiment applied to MODE-73. *Deep-Sea Res. Oceanogr. Abstr.*, **23**, 559–582, doi:10.1016/0011-7471(76)90001-2.

Cazenave, A., and Coauthors, 2012: Estimating ENSO influence on the global mean sea level, 1993–2010. *Mar. Geod.*, **35** (Suppl.), 82–97, doi:10.1080/01490419.2012.718209.

Chang, Y.-S., and H.-R. Shin, 2014: Vertical gradient correction for the oceanographic atlas of the East Asian seas. *J. Geophys. Res. Oceans*, **119**, 5546–5554, doi:10.1002/2014JC009845.

——, A. J. Rosati, and G. A. Vecchi, 2010: Basin patterns of global sea level changes for 2004–2007. *J. Mar. Syst.*, **80**, 115–124, doi:10.1016/j.jmarsys.2009.11.003.

——, G. A. Vecchi, A. Rosati, S. Zhang, and X. Yang, 2014: Comparison of global objective analyzed T-S fields of the upper ocean for 2008–2011. *J. Mar. Syst.*, **137**, 13–20, doi:10.1016/j.jmarsys.2014.04.001.

Delcroix, T., G. Alory, S. Cravatte, T. Corrège, and M. McPhaden, 2011: A gridded sea surface salinity data set for the tropical

Pacific with sample applications (1950–2008). *Deep-Sea Res. I*, **58**, 38–48, doi:10.1016/j.dsr.2010.11.002.

Desbruyères, D., V. Thierry, and H. Mercier, 2013: Simulated decadal variability of the meridional overturning circulation across the A25-Ovide section. *J. Geophys. Res. Oceans*, **118**, 462–475, doi:10.1029/2012JC008342.

Domingues, C. M., J. A. Church, N. J. White, P. J. Gleckler, S. E. Wijffels, P. M. Barker, and J. R. Dunn, 2008: Improved estimates of upper-ocean warming and multi-decadal sea-level rise. *Nature*, **453**, 1090–1093, doi:10.1038/nature07080.

Freeland, H. J., and Coauthors, 2010: Argo—A decade of progress. *Proc. OceanObs'09: Sustained Ocean Observations and Information for Society*, Venice, Italy, Vol. 2, European Space Agency, 14 pp., doi:10.5270/OceanObs09.cwp.32.

Gaillard, F., 2012: ISAS-tool version 6: Method and configuration. Ifremer Tech. Rep. LPO-12-02, 18 pp., doi:10.13155/22583.

——, E. Autret, V. Thierry, P. Galaup, C. Coatanoan, and T. Loubrieu, 2009: Quality control of large Argo datasets. *J. Atmos. Oceanic Technol.*, **26**, 337–351, doi:10.1175/2008JTECHO552.1.

Hood, M., and Coauthors, 2010: Ship-based repeat hydrography: A strategy for a sustained global program. *Proc. OceanObs'09: Sustained Ocean Observations and Information for Society*, Venice, Italy, Vol. 2, European Space Agency, 11 pp., doi:10.5270/OceanObs09.cwp.44.

Ide, K., P. Courtier, M. Ghil, and A. C. Lorenc, 1997: Unified notation for data assimilation: Operational, sequential and variational. *J. Meteor. Soc. Japan*, **75**, 181–189.

Kim, W., S.-W. Yeh, J.-H. Kim, J.-S. Kug, and M. Kwon, 2011: The unique 2009–2010 El Niño event: A fast phase transition of warm pool El Niño to La Niña. *Geophys. Res. Lett.*, **38**, L15809, doi:10.1029/2011GL048521.

Kolodziejczyk, N., and F. Gaillard, 2013: Variability of the heat and salt budget in the subtropical southeastern Pacific mixed layer between 2004 and 2010: Spice injection mechanism. *J. Phys. Oceanogr.*, **43**, 1880–1898, doi:10.1175/JPO-D-13-04.1.

Lee, T., and M. J. McPhaden, 2008: Decadal phase change in large-scale sea level and winds in the Indo-Pacific region at the end of the 20th century. *Geophys. Res. Lett.*, **35**, L01605, doi:10.1029/2007GL032419.

Levitus, S., and Coauthors, 2012: World ocean heat content and thermosteric sea level change (0–2000 m), 1955–2010. *Geophys. Res. Lett.*, **39**, L10603, doi:10.1029/2012GL051106.

Locarnini, R. A., A. V. Mishonov, J. I. Antonov, T. P. P. Boyer, and H. E. Garcia, 2010: *Temperature*. Vol. 1, *World Ocean Atlas 2009*, NOAA Atlas NESDIS 68, 184 pp. [Available online at ftp://ftp.nodc.noaa.gov/pub/WOA09/DOC/woa09_vol1_text.pdf.]

——, and Coauthors, 2013: *Temperature*. Vol. 1, *World Ocean Atlas 2013*, NOAA Atlas NESDIS 73, 40 pp. [Available online at http://data.nodc.noaa.gov/woa/WOA13/DOC/woa13_vol1.pdf.]

Lyman, J. M., and G. C. Johnson, 2008: Estimating annual global upper-ocean heat content anomalies despite irregular in situ ocean sampling. *J. Climate*, **21**, 5629–5641, doi:10.1175/2008JCLI2259.1.

——, S. A. Good, V. V. Gouretski, M. Ishii, G. C. Johnson, M. D. Palmer, D. M. Smith, and J. K. Willis, 2010: Robust warming of the global upper ocean. *Nature*, **465**, 334–337, doi:10.1038/nature09043.

Mercier, H., and Coauthors, 2015: Variability of the meridional overturning circulation at the Greenland–Portugal OVIDE section from 1993 to 2010. *Prog. Oceanogr.*, **132**, 250–261, doi:10.1016/j.pocean.2013.11.001.

Meyssignac, B., and A. Cazenave, 2012: Sea level: A review of present-day and recent-past changes and variability. *J. Geodyn.*, **58**, 96–109, doi:10.1016/j.jog.2012.03.005.

Morrow, R., and E. Kestenare, 2014: Nineteen-year changes in surface salinity in the Southern Ocean south of Australia. *J. Mar. Syst.*, **129**, 472–483, doi:10.1016/j.jmarsys.2013.09.011.

Roemmich, D., and J. Gilson, 2009: The 2004–2008 mean and annual cycle of temperature, salinity, and steric height in the global ocean from the Argo program. *Prog. Oceanogr.*, **82**, 81–100, doi:10.1016/j.pocean.2009.03.004.

——, and ——, 2011: The global ocean imprint of ENSO. *Geophys. Res. Lett.*, **38**, L13606, doi:10.1029/2011GL047992.

Roquet, F., J.-B. Charrassin, S. Marchand, L. Boehme, M. Fedak, G. Reverdin, and C. Guinet, 2011: Delayed-mode calibration of hydrographic data obtained from animal-borne satellite relay data loggers. *J. Atmos. Oceanic Technol.*, **28**, 787–801, doi:10.1175/2010JTECHO801.1.

Rusciano, E., S. Speich, and M. Ollitrault, 2012: Interocean exchanges and the spreading of Antarctic Intermediate Water south of Africa. *J. Geophys. Res. Oceans*, **117**, C10010, doi:10.1029/2012JC008266.

Sarafanov, A. A., A. V. Sokov, and A. S. Falina, 2009: Warming and salinification of Labrador Sea Water and deep waters in the subpolar North Atlantic at 60°N in 1997–2006. *Oceanology*, **49**, 193–204, doi:10.1134/S0001437009020040.

von Schuckmann, K., F. Gaillard, and P.-Y. Le Traon, 2009: Global hydrographic variability patterns during 2003–2008. *J. Geophys. Res.*, **114**, C09007, doi:10.1029/2008JC005237.

Willis, J. K., D. P. Chambers, and R. S. Nerem, 2008: Assessing the globally averaged sea level budget on seasonal to interannual timescales. *J. Geophys. Res.*, **113**, C06015, doi:10.1029/2007JC004517.

Yu, J.-Y., and S. T. Kim, 2013: Identifying the types of major El Niño events since 1870. *Int. J. Climatol.*, **33**, 2105–2112, doi:10.1002/joc.3575.

Zilberman, N. V., D. H. Roemmich, and S. T. Gille, 2014: Meridional volume transport in the South Pacific: Mean and SAM-related variability. *J. Geophys. Res. Oceans*, **119**, 2658–2678, doi:10.1002/2013JC009688.

Zunino, P., M. Vargas-Yáñez, F. Moya, M. C. García-Martínez, and F. Plaza, 2009: Deep and intermediate layer warming in the western Mediterranean: Water mass changes and heaving. *Geophys. Res. Lett.*, **36**, L20608, doi:10.1029/2009GL039578.